Surface Science 220 (1989) 96–117
North-Holland, Amsterdam

LOW TEMPERATURE SURFACE DIFFUSION AND DECOMPOSITION OF $[Rh(CO)_2Cl]_2$ ADSORBED ON OXIDIZED Al(100)

David N. BELTON and Craig L. DIMAGGIO

Physical Chemistry Department, General Motors Research Laboratories, Warren, MI 48090, USA

Received 9 February 1989; accepted for publication 3 May 1989

The adsorption and decomposition of $[Rh(CO)_2Cl]_2$ on three different model Al_2O_3 supports were studied with high resolution electron energy loss spectroscopy (HREELS) and temperature programmed desorption (TPD). The aluminum oxide supports were prepared by oxidation of Al(100) single crystal with either oxygen or water at temperatures from 425 to 725 K to prepare Al_2O_3 films of three types: planar-dehydroxylated, porous-dehydroxylated, and planar-hydroxylated. TPD of adsorbed $[Rh(CO)_2Cl]_2$ showed that $[Rh(CO)_2Cl]_2$ decomposed on the Al_2O surfaces above 275 K and that the decomposition kinetics were dependent on the substrate porosity. HREELS data showed that on the porous Al_2O_3 layers, $[Rh(CO)_2Cl]_2$ diffuses to stable binding sites within the pore structure below 245 K after which decomposition proceeds. For $[Rh(CO)_2Cl]_2$ on hydroxylated Al_2O_3 films changes in the OH stretch region of the HREELS spectrum indicate that $[Rh(CO)_2Cl]_2$ reacts with surface OH groups below 275 K. The experiments demonstrate that HREELS can be applied to the study of adsorbates on oxide supports in spite of complications of strong oxide lattice modes and poor resolution due to the nature of the support.

1. Introduction

Noble metals supported on aluminum oxide are currently the most active catalysts for many important processes including the reduction of pollutants in automobile exhaust [1–4]. A fundamental understanding of reaction rates and mechanisms over conventional supported catalysts is elusive because of the inherent difficulty of identifying and quantifying the active sites for a catalyst with a complicated manifold of particle sizes and compositions. The complexity of practical catalysts entices investigators to seek out simpler model systems that can be more readily understood. Progress toward a detailed understanding of the effect of composition and structure on reactivity has been forthcoming from research in two complementary areas: combined ultra-high vacuum (UHV)–moderate pressure reactor studies on single crystal metals [5–7] and in situ infrared investigations of adsorbed reactants on supported metals at moderate (1–100 Torr) pressure [8–11]. The single crystal research has been important for identification of adsorption energies, bonding

0039-6028/89/$03.50

geometries and reaction kinetics. IR studies on supported catalysts have identified adsorption sites, monitored surface coverages, measured reaction kinetics and observed structural changes in the metal particles. The IR investigations are especially informative when inorganic cluster compounds of known structure are anchored on the support intact giving the experiment a well defined starting material, as opposed to the particle size distribution typical in conventional catalysts [12–14]. Although quite powerful in their ability to define and monitor adsorption sites, especially for CO, IR studies sometime lack supporting evidence to confirm proposed structures based on vibrational spectroscopy alone. In this study we combine the surface analytical techniques of Auger electron spectroscopy (AES), temperature programmed desorption (TPD), and high resolution electron energy loss spectroscopy (HREELS) to study the adsorption behavior of one inorganic precursor, $[Rh(CO)_2Cl]_2$, on aluminum oxide.

Previously, we have investigated the thermal behavior of $[Rh(CO)_2Cl]_2$ on oxidized Al(100) using X-ray photoelectron spectroscopy (XPS), AES, and TPD [15]. That work demonstrated the potential usefulness of surface analysis for the in situ examination of the preparation of model catalysts under UHV conditions. $[Rh(CO)_2Cl]_2$ is one of the most studied Rh carbonyl compounds, because of its air stability, commercial availability, and amenable vapor pressure. Many IR investigations of $[Rh(CO)_2Cl]_2$ supported on Al_2O_3 and SiO_2 have appeared, mostly showing that the molecule can be adsorbed on the support intact below room temperature and that decomposition of reaction occurs at elevated temperatures [16–18]. Some work in vacuum has also been carried out by Bowser and Weinberg using inelastic electron tunneling spectroscopy (IETS) [19], and by Frederick et al. using XPS [20]. In both cases decomposition of the molecule at elevated temperatures was demonstrated. In our earlier paper we showed that the decomposition kinetics of $[Rh(CO)_2Cl]_2$ on oxidized Al(100) were dependent on the structure of the Al_2O_3 support [15]. On thin planar oxide films $[Rh(CO)_2Cl]_2$ decomposed via a pathway we characterized as being most similar to bulk $[Rh(CO)_2Cl]_2$ decomposition which lead to relatively large (120 Å) Rh crystallites. However, for much thicker Al_2O_3 supports with substantial quantities of subsurface pores the decomposition pathway was markedly different. For the porous supports, we characterized the mechanism as molecular $[Rh(CO)_2Cl]_2$ decomposition which resulted in the formation of much smaller (20 Å) Rh particles. In that paper [15] we postulated that the $[Rh(CO)_2Cl]_2$ diffused to stable binding sites within the pores below room temperature where agglomeration of $[Rh(CO)_2Cl]_2$ into large crystallites was inhibited. Thus, these undefined sites within the pore structure stabilized much smaller Rh particles than were obtainable on the more planar surfaces. The proposed mechanisms were based on the decomposition kinetics for $[Rh(CO)_2Cl]_2$ and on XPS, AES, and CO TPD measurements which showed large differences in Rh particle sizes after $[Rh(CO)_2Cl]_2$

decomposition. This study raised questions that could not be answered in the system used for the XPS–TPD study.

The HREELS investigation reported here was undertaken in an effort to obtain more detailed information about the decomposition mechanism of $[Rh(CO)_2Cl]_2$. With its relatively low cutoff of about 200 cm^{-1} HREELS has, in theory, the ability to examine the Rh–Cl stretch and monitor the scission of this bond. Also, we wanted to observe more directly the low temperature mobility of $[Rh(CO)_2Cl]_2$ to confirm this aspect of our proposed mechanism for $[Rh(CO)_2Cl]_2$ decomposition on porous Al_2O_3 films. This HREELS investigation was also motivated by some unpublished results which showed no effect of surface hydroxyl species on the decomposition of $[Rh(CO)_2Cl]_2$; however, that work was compromised by our limited ability to identify surface OH species via XPS. HREELS offers a vibrational identification of OH on the support and thus allows a more positive statement as to its effect on $[Rh(CO)_2Cl]_2$ chemistry. Finally, we wanted to use this experiment to test the usefulness of HREELS for the study of supported metal particles. Studying $[Rh(CO)_2Cl]_2$, with its known structure and IR spectrum with bands between about 300 and 2100 cm^{-1}, affords us a good assessment of the utility of HREELS for supported metals.

2. Experimental aspects

The experiments were performed in a standard ion-pumped UHV system with capability for HREELS, TPD, AES, and LEED similar to that described elsewhere [21]. The system was equipped with microchannel array dosers that facilitated controlled exposures of $[Rh(CO)_2Cl]_2$ onto the oxidized Al(100) sample. The details of $[Rh(CO)_2Cl]_2$ dosing were reported earlier [22] and will not be repeated at length here; however, from the combination of TPD and XPS results reported before, we are confident that $[Rh(CO)_2Cl]_2$ was delivered to the sample without the loss of CO. Desorptions were done with an apertured quadrupole mass spectrometer to inhibit detection of desorption from surfaces other than the crystal face. The sample manipulator on which the Al(100) crystal was mounted was equipped with resistive heating and liquid N_2 cooling. The Al crystal was oriented to within 1° and polished to a mirror finish with 1 μm diamond paste prior to introduction into the vacuum system. The sample was cleaned of all carbon contamination and most of the oxygen contamination prior to oxidation to form the Al_2O_3 overlayers used as substrates for these experiments. For preparation of the films examined here, the Al(100) was exposed to approximately 10^{-6} Torr of O_2 for 30 min at temperatures between 425 and 725 K. The oxidation of Al(100) is addressed in further detail in the results section.

3. Results

3.1. Oxidation of Al(100)

The purpose of these experiments was to examine the temperature dependent behavior of $[Rh(CO)_2Cl]_2$ on three different aluminum oxide surfaces: planar-dehydroxylated, porous-dehydroxylated, and planar-hydroxylated. The Al_2O_3 films were prepared under UHV conditions after cleaning the sample of impurities by Ar^+ ion bombardment and annealing cycles. The hydroxylated planar films were made by oxidizing the clean Al(100) with 5×10^{-6} Torr of O_2 at 575 K for 30 min (9000 L). The dehydroxylated porous Al_2O_3 films were prepared by using the same exposure (9000 L) at a higher temperature, 725 K. The presence of subsurface pores was previously demonstrated using a combination of XPS and TPD [15] and is substantiated by the HREELS data of this paper. The hydroxylated planar Al_2O_3 substrates were prepared by exposure to 1000 L of water at 425 K. Previous studies have shown that oxidation of Al(100) with water leads to formation of surface hydroxyls [23–26] and that water oxides Al faster than oxygen [24].

Based on the Auger spectra taken after oxidation of the Al(100) crystal we estimate the Al_2O_3 thicknesses to be 20 Å for the planar films and greater than 30 Å for the porous films. For these experiments quantification of the layer thickness is not as important as estimating the amount of Al^0 present at the surface of the sample over the temperature range of interest. It has been shown rather convincingly that Al_2O_3 films prepared by UHV oxidation can have significant amounts of metallic Al at the surface and distributed within the film [24,26]. It turns out that the decomposition of $[Rh(CO)_2Cl]_2$ is also very sensitive to the presence of metallic Al at the surface of the oxidized Al(100) crystal [27]. When Al metal interacts with $[Rh(CO)_2Cl]_2$ above 300 K, CO dissociates on the substrate causing a large C Auger signal; however, when only oxidized Al is present at the surface no CO dissociation occurs and decarbonylation of $[Rh(CO)_2Cl]_2$ occurs via CO desorption. By checking the Auger spectrum after a set of HREELS experiments, it was possible to tell if metallic aluminum was generated at the surface over the temperature range studied. The tendency of Al^0 to migrate to the surface at relatively low temperatures (400 K) for very thin Al_2O_3 layers forced us to select somewhat more vigorous oxidation conditions than were optimal for obtaining the highest quality HREELS data.

3.2. Adsorption / desorption of $[Rh(CO)_2Cl]_2$

Once a particular Al_2O_3 film was prepared, the substrate ($T = 110$ K) was exposed to $[Rh(CO)_2Cl]_2$. $[Rh(CO)_2Cl]_2$ adsorbs molecularly at 110 K when proper care is taken to assure that molecular $[Rh(CO)_2Cl]_2$ is arriving at the

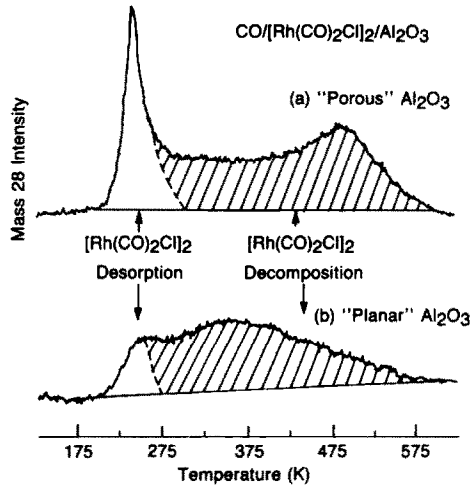

Fig. 1. Mass 28 TPD of a multilayer $[Rh(CO)_2Cl]_2$ exposure on (a) a porous Al_2O_3 film on Al(100) and (b) a planar Al_2O_3 film. The low temperature peak is from cracking of molecular $[Rh(CO)_2Cl]_2$ in the QMS with the broader high temperature peak from surface decomposition of $[Rh(CO)_2Cl]_2$.

surface of the sample. The details of $[Rh(CO)_2Cl]_2$ dosing were the subject of a previous paper [22] and were also addressed by Frederick et al. [20]. TPD of an adsorbed multilayer deposit is quite helpful for establishing the pertinent temperature range to examine $[Rh(CO)_2Cl]_2$ decomposition with HREELS. Fig. 1 shows the TPD spectrum for multilayer $[Rh(CO)_2Cl]_2$ adsorbed onto both porous (fig. 1a) and planar (fig. 1b) dehydroxylated Al_2O_3 films, although in fig. 1b the exposure was lower. Data for desorption from the planar hydroxylated Al_2O_3 layers are indistinguishable from the corresponding data of planar OH free surfaces (fig. 1b). The obvious differences in the desorption spectra from the two surfaces were the motivation for the HREELS investigation reported here. Examining the porous film (fig. 1a) first, we observed two features of different origin when mass 28 was monitored as a function of temperature. The data were obtained by multiplexing 9 masses simultaneously which allowed us to make the following assignments of the two peaks. The sharper low temperature peak showed zero order desorption kinetics as a function of $[Rh(CO)_2Cl]_2$ exposure and did not saturate for very large (1000 $\times$ greater than fig. 1) exposures. Zero order desorption kinetics suggest that the low temperature peak is due to desorption of a condensed phase, presumably $[Rh(CO)_2Cl]_2$. When other masses (i.e., 35, 37, 103, 131, etc.) were examined, it was determined that the entire cracking pattern of molecular $[Rh(CO)_2Cl]_2$ was observable at this same temperature. This observation proves that the low temperature peak is due to cracking of $[Rh(CO)_2Cl]_2$ in the mass spectrometer

during desorption of molecular $[Rh(CO)_2Cl]_2$. In contrast, no Rh or Cl containing species were detected concurrent with the higher temperature mass 28 desorption peak; therefore, we assigned this peak to evolution of CO as a product of $[Rh(CO)_2Cl]_2$ decomposition. Turning now the desorption from the planar substrate, fig. 1b shows the differences in decomposition profile that are the subject of the HREELS investigation. The molecular desorption peak at low temperature, less resolved here because of the lower $[Rh(CO)_2Cl]_2$ exposure, is the same as on the porous surface; however, the peak from the surface decomposition of $[Rh(CO)_2Cl]_2$ has a maximum about 110 K lower than on the porous sample. The HREELS experiments that follow probe this difference by examining the vibrational spectrum for adsorbed $[Rh(CO)_2Cl]_2$ as a function of temperature.

3.3. HREELS of $[Rh(CO)_2Cl]_2$ on planar Al_2O_3

This section examines HREELS of submonolayer and multilayer $[Rh(CO)_2Cl]_2$ coverages on the simplest oxide support, planar dehydroxylated Al_2O_3. The $[Rh(CO)_2Cl]_2$ coverage was calibrated by examining the area under the low temperature (multilayer) desorption peak (fig. 1). Exact quantification of the coverage was difficult due to irreproducibility in the flux from the doser and overlap in the TPD peaks of fig. 1; however, we could easily deposit either multilayer or submonolayer quantities of $[Rh(CO)_2Cl]_2$. Prior to $[Rh(CO)_2Cl]_2$ exposure the Al_2O_3 film was characterized with HREELS (fig. 2a) using a 2.7 eV primary beam and monitoring losses in the specular direction. The data show three major losses at 470, 650, and 875 cm^{-1} for the Al_2O_3 film on Al(100) in agreement with previous studies [25,28,29]. The peaks have been assigned to lattice vibrations in the Al_2O_3 film. The modes at 470 and 875 cm^{-1} are due to bulk Al–O vibrations and the loss at 650 cm^{-1} is assigned to a surface Al–O mode [25,28,29]. At higher wavenumbers the harmonics of these strong modes were also detected and can be seen as a small peak just below 2000 cm^{-1}. These Al_2O_3 modes are very strong and, as evidenced in fig. 2b, have significant overlap with the modes of $[Rh(RO)_2Cl]_2$.

The data of fig. 2b, taken at 110 K, show the appearance of several new losses upon adsorption of $[Rh(CO)_2Cl]_2$. The strongest loss, marked as a doublet at 2065 and 2100 cm^{-1} is due to the CO stretch of the Rh dicarbonyl species. The assignment of a doublet is based on our previous observation of molecular $[Rh(CO)_2Cl]_2$ adsorption at 110 K and the known IR spectrum of $[Rh(CO)_2Cl]_2$ [30]. The inability to fully resolve these two peaks is due to the limited resolution of HREELS and to the further degradation of that resolution on these oxide substrates. In addition to the CO stretch, four modes were detected below 1000 cm^{-1} in fig. 2b. The peak at 870 cm^{-1} is attributed to Al_2O_3 lattice vibration, shifted slightly after adsorption of $[Rh(CO)_2Cl]_2$; however, the other three modes can be assigned to adsorbed $[Rh(CO)_2Cl]_2$

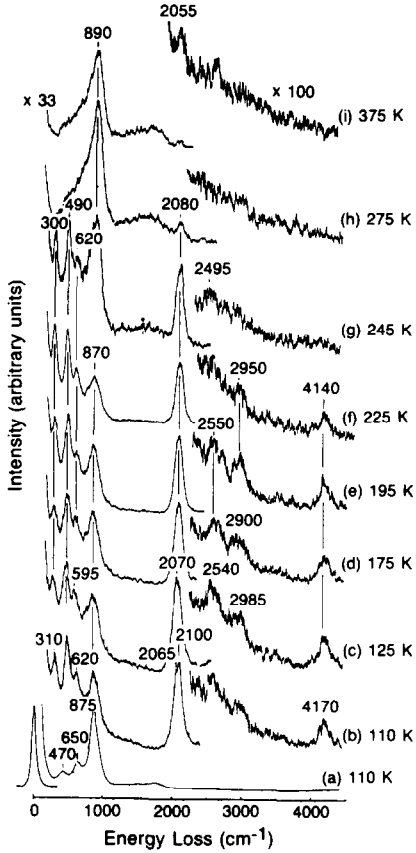

Fig. 2. HREELS of a multilayer $[Rh(CO)_2Cl]_2$ deposit on a planar Al_2O_3 film prepared by oxidation of Al(100) with O_2 at 575 K. HREELS data were obtained with a 2.7 eV primary beam with losses monitored in the specular direction. Sample was annealed to successively higher temperature and then cooled to 110 K prior to taking the HREELS spectrum.

[30]. The assignments of the $[Rh(CO)_2Cl]_2$ vibrations (table 1) are based on solution and gas phase IR data of $[Rh(CO)_2Cl]_2$ [30] by Garland and Wilt. The stretch we observed at 620 cm^{-1} was seen by Garland and Wilt at 610 cm^{-1}; however, they did not assign the mode. In that paper [30] they showed that the 610 cm^{-1} mode only shifted 11 cm^{-1} upon substitution of Br for Cl in $[Rh(CO)_2Cl]_2$, suggesting that the peak is due to a Rh–CO type mode, possibly a bending mode. The weak stretching mode observed at 4170 cm^{-1} is assigned as a harmonic of the very strong CO stretching mode centered at 2080 cm^{-1}. From our point of view the most interesting mode to examine as a function of temperature is the Rh–Cl stretch at 310 cm^{-1}.

Table 1
Assignment of loss features for $[Rh(CO)_2Cl]_2$ on oxidized Al(100)

Assignment	This work (cm^{-1})	Lit. value (cm^{-1})	Ref.
Rh–Cl	310	260 vs, 274 vs, 300 sh	[30]
Al–O (bulk)	470	430 m	[25,28,29]
Rh–CO	490	435 m or 485 m	[30] or [32]
Rh–CO bend (?)	620	610 m	[30]
Al–O (surface)	650	650 m	[25,28,29]
Al–O (bulk)	875	870 s	[25,28,29]
$Rh–(CO)_2$ (sym+asym)	2070	2095 s and 2043 s	[30]
Al–O (harmonic-875)	2540	–	[25,28,29]
Comb. band (875+2070)	2985	–	–
$Rh–(CO)_2$ harmonic	4140	–	–

After characterization of the multilayer deposit at 110 K, the sample was annealed to successively higher temperatures, cooled to 110 K and HREELS spectra obtained. The anneal to 125 K produced no observable change in the region below 2000 cm^{-1} and only a slight shift in the centroid of the CO stretch at 2080 cm^{-1}. In fig. 2c the CO stretching region is labeled as a single peak, which is probably the most consistent way to assign this mode. Another minor change in the data is a 30 cm^{-1} shift of the 4170 cm^{-1} peak to 4140 cm^{-1} with some narrowing in the peak width. Also, this spectrum (fig. 2c) labels two new modes at 2540 cm^{-1} and 2985 cm^{-1}. The mode at 2540 cm^{-1} is almost certainly the second harmonic of the lattice mode at 875 cm^{-1} (see fig. 2a). The mode at 2985 cm^{-1} is not so easily assigned since its intensity is small and rises and falls with the intensity of the CO stretch but, we assign this peak as a combination band (C–O stretch, 2080 cm^{-1}, +Al–O, 875 cm^{-1}).

The first substantial change in the HREELS data was observed when the sample was heated to 245 K before acquisition of the spectrum (fig. 2g). Between the 225 and 245 K the mode at 4140 cm^{-1} disappeared, the mode at 870 cm^{-1} became much more pronounced, the CO stretch at 2080 cm^{-1} decreased in intensity, and the peak at 2950 cm^{-1} is gone. The TPD data of fig. 1 show that 245 K is on the leading edge of the multilayer desorption peak, but that substantial amounts of condensed $[Rh(CO)_2Cl]_2$ remain on the surface at 245 K consistent with the HREELS data (fig. 2g). Dramatic changes in all regions of the data occur when the sample temperature was raised to 275 K. Primarily, almost all of the intensity in the CO stretching mode (2080 cm^{-1}) was lost making the Al_2O_3 lattice vibration at 890 cm^{-1} the strongest mode in the spectrum. Desorption of the condensed $[Rh(CO)_2Cl]_2$ multilayer is complete at 275 K; therefore, all of the $[Rh(CO)_2Cl]_2$ stretching modes drop sharply when the surface $[Rh(CO)_2Cl]_2$ concentration is reduced. For temperatures above 275 K the CO stretch intensity drops and the peak shifts to 2055

cm^{-1} (fig. 2i). The observed peak shift is consistent with the generation of different adsorbed CO species upon $[Rh(CO)_2Cl]_2$ decomposition.

The data of fig. 2 showed that most of the action occurs near the desorption temperature of multilayer $[Rh(CO)_2Cl]_2$. Because condensed $[Rh(CO)_2Cl]_2$ covers the surface until the multilayer desorbs, interpretation of the HREELS data for the adsorbed monolayer at temperatures below 275 K is impossible. This problem can be eliminated by adsorbing submonolayer amounts of $[Rh(CO)_2Cl]_2$ for which very little or no desorption of *molecular* $[Rh(CO)_2Cl]_2$ occurs. Instead, only CO desorption from $[Rh(CO)_2Cl]_2$ decomposition occurs in the temperature region above 275 K. Fig. 3 shows the data set for submonolayer $[Rh(CO)_2Cl]_2$ on planar Al_2O_3. The data were obtained in exactly the same manner as for the multilayer deposit shown in fig. 2. The Al(100) sample was cleaned of all Rh, Cl and O prior to oxidation to form an Al_2O_3 layer in the same manner as the previous sample. Again, the spectrum for the clean substrate is shown in fig. 3a, with the region for the first harmonic expanded. The data agree very well with their counterpart in fig. 2a.

When the sample was exposed to a submonolayer quantity of $[Rh(CO)_2Cl]_2$ at 110 K, the spectrum shown in fig. 3b was obtained. The data show only one new feature upon adsorption of $[Rh(CO)_2Cl]_2$, the overlapping symmetric and asymmetric CO stretches centered at 2075 cm^{-1}. Relative to fig. 2 the low intensity of the CO stretch and the high intensity of the first harmonics of the substrate modes (1200–1800 cm^{-1}) shows that the $[Rh(CO)_2Cl]_2$ coverage is significantly less than for the case presented in fig. 2. The $[Rh(CO)_2Cl]_2$ modes at 310 and 490 cm^{-1} are not observed for the adsorbed monolayer; however, based on their intensities relative to that for the CO stretch (fig. 2b) they should be obscured by the Al_2O_3 modes at this $[Rh(CO)_2Cl]_2$ coverage. The other change in the data after $[Rh(CO)_2Cl]_2$ adsorption is that the Al_2O_3 modes become less clearly defined; this effect is most evident for the harmonics between 1200 and 1800 cm^{-1}.

When the sample was annealed to successively higher temperatures, the first significant change in the HREELS spectrum occurred between 175 and 200 K. By 200 K changes in the resolution and intensity of the low wavenumber Al_2O_3 modes are clearly evident and the CO stretch intensity increased by about 40% over that observed at 110 K. Above 200 K the CO stretch intensity declines similar to the multilayer deposit; however, on this sample (fig. 3) no desorption of molecular $[Rh(CO)_2Cl]_2$ occurs. About half of the initial CO stretch intensity is lost by 275 K and the surface Al–O mode at 640 cm^{-1} is detected as a shoulder on the peak at 895 cm^{-1}. As the sample is annealed to higher temperature the CO stretch intensity decreases further and a shift to lower wavenumbers (2050 cm^{-1}) is observed. The data show that two distinctly different events are occurring on the surface. Below 275 K intensity changes but the peak position is constant indicating a rearrangement of the adsorbed layer while the $[Rh(CO)_2Cl]_2$ structure is maintained. Above 275 K

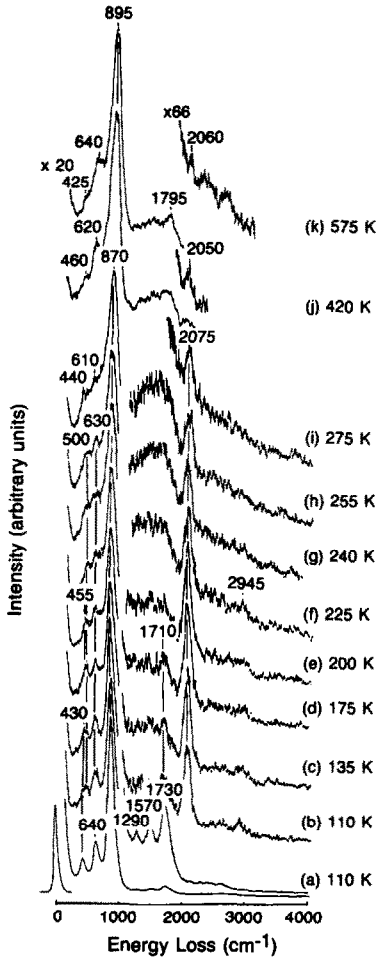

Fig. 3. HREELS of a submonolayer $[Rh(CO)_2Cl]_2$ deposit on a planar Al_2O_3 film prepared by oxidation of Al(100) with O_2 at 575 K. Data were taken with a 2.7 eV primary beam using specular reflection. The sample was heated to the indicated temperature then cooled to 110 K prior to obtaining the HREELS spectrum.

the intensity drops and the peak shifts to lower wavenumbers suggesting both a loss of CO from the surface and a change in the nature of the CO adsorption site.

3.4. HREELS of $[Rh(CO)_2Cl]_2$ on "porous" Al_2O_3

As stated previously, our goal is to examine the decomposition of $[Rh(CO)_2Cl]_2$ on oxide substrates that have exhibited different TPD decom-

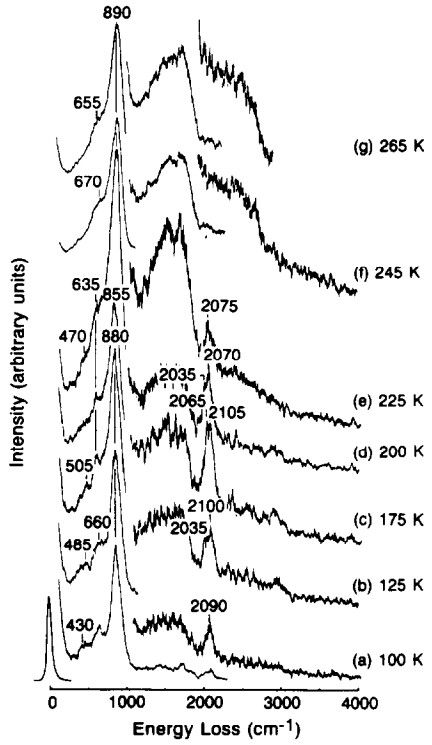

Fig. 4. HREELS of a submonolayer $[Rh(CO)_2Cl]_2$ deposit on a *porous* Al_2O_3 film prepared by oxidation of Al(100) with O_2 at 725 K. Data were obtained at 110 K after heating to the specified temperatures.

position profiles (fig. 1). This section will examine the HREELS data on the porous Al_2O_3 substrate discussed in section 3.1. HREELS data for submonolayer and multilayer quantities of $[Rh(CO)_2Cl]_2$ on a porous Al_2O_3 support were obtained. Data for multilayers of $[Rh(CO)_2Cl]_2$ on the porous Al_2O_3 substrate were essentially the same as on the planar film (fig. 2a) below 250 K (prior to desorption of the condensed phase); therefore, we present only the data for the submonolayer exposure (fig. 4). Data from the clean substrate are ommitted from fig. 4; however, the same lattice Al_2O_3 modes were observed as for the planar films. In this case the overall resolution and signal intensity were degraded slightly on the thicker oxide overlayer. The elastic peak shown in fig. 4 is about 20 cm^{-1} wider than for the case of the planar film, but this did not seriously limit the usefulness of the data obtained from this sample. The data (fig. 4) were taken in the same manner as for the two preceding samples; however, for this particular experiment our minimum temperature was 100 K. The best comparison for this data would be to the submonolayer

data of fig. 3. Similar to fig. 3 we see an increase in CO stretch intensity and resolution between 100 and 175 K. Also similar to the planar sample is the degradation of Al_2O_3 modes upon adsorption at low temperatures; however, in this case the modes are never clearly resolved even for the clean substrate. The main difference between figs. 3 and 4 is that all of the CO stretch intensity is gone at 245 K on porous Al_2O_3 (fig. 4) and no shift in CO stretching frequency was observed.

3.5. HREELS of $[Rh(CO)_2Cl]_2$ on planar hydroxylated Al_2O_3

Another question about the interaction of $[Rh(CO)_2Cl]_2$ with Al_2O_3 surfaces arose when, in a previous unpublished experiment, we observed no effect of surface hydroxyls on the $[Rh(CO)_2Cl]_2$ TPD spectrum (fi. 1). Several authors have demonstrated that hydroxylated Al_2O_3 surfaces can be prepared in UHV by treatment of Al with water [23–26]. The hydroxylated Al_2O_3 surfaces was prepared by oxidation of the Al(100) crystal with water at 425 K. The HREELS spectrum of the surface prepared in this manner is shown in fig. 5a where the O–H stretch is identified at 3700 cm^{-1} [25]. The Al_2O_3 lattice modes are also evident at similar frequencies to those for dehydroxylated Al_2O_3 layers and is in good agreement with published data for Al_2O_3 films prepared in this manner [25].

Upon exposure to a submonolayer amount of $[Rh(CO)_2Cl]_2$ (fig. 5b), the O–H stretch at 3700 cm^{-1} becomes obscured. The CO stretch at about 2070 cm^{-1} is clearly visible and with faith the Rh–CO mode at 480 cm^{-1} can be identified. When the sample is annealed to 125 K, the Rh–CO mode becomes more easily discernible. The linear fall off between 3000 and 3500 cm^{-1} is the third harmonic of the Al_2O_3 mode at 890 K, which means that the O–H stretch is not detectable. As the sample temperature is raised the CO stretch fades slightly at 200 K and at no temperature is the Rh–Cl stretch detected, as expected from the relative intensities of the $[Rh(CO)_2Cl]_2$ modes as observed for the multilayer $[Rh(CO)_2Cl]_2$ deposit in fig. 2. By a temperature of 265 K the CO stretch has decreased significantly as was observed in the other four samples. Also, at 265 K the shape of the region above 3500 cm^{-1} showed significantly more intensity around 3700 cm^{-1}. As the sample is annealed above 275 K the CO stretch decreases in intensity and shifts in the same manner as on the planar dehydroxylated film.

With regards to the OH stretch, the data are not so clear due to several factors which, in combination, make the interpretation of the OH stretch region difficult. First, the OH intensity is very low; whether the concentration is low or the extinction coefficient poor is not clear. Second, this weak transition overlaps with a harmonic of the lattice vibration modes raising the background in the area of the small OH peak. Regardless of these problems we definitely see changes in the OH region as a function of temperature after

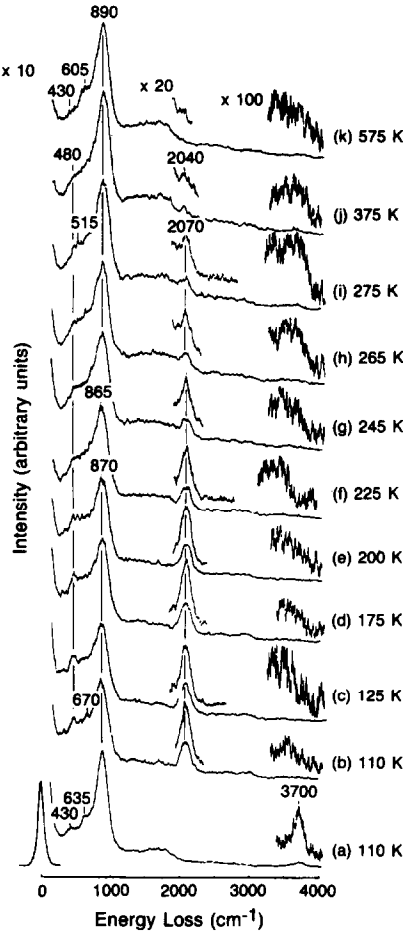

Fig. 5. HREELS of a submonolayer $[Rh(CO)_2Cl]_2$ deposit on a hydroxylated planar Al_2O_3 film prepared by oxidation of Al(100) with water at 425 K. Data were obtained at 100 K after annealing the sample to the specified temperature.

deposition of $[Rh(CO)_2Cl]_2$. In a separate experiment we demonstrated that the OH species were stable above 400 K in the absence of $[Rh(CO)_2Cl]_2$ when the surface was oxidized at 400 K with water. This leads us to conclude that some interaction of OH and $[Rh(CO)_2Cl]_2$ is occurring. This interaction does not, however, grossly change the decomposition profile as evidenced by TPD or HREELS. A simple explanation based on chemical intuition is that the hydroxyls react with Cl in $[Rh(CO)_2Cl]_2$ and are eliminated as HCl; however, this simple picture is not proven on the basis of our HREELS data.

4. Discussion

This paper examines the thermal behavior of $[Rh(CO)_2Cl]_2$ on oxidized Al(100) prepared to give three different oxide supports: planar without hydroxyls, porous without hydroxyls, and planar with hydroxyls. The experiment also compare two different initial $[Rh(CO)_2Cl]_2$ coverages, multilayers and submonolayer, on the supports. The results are most easily summarized by first comparing submonolayer and multilayer exposures on a planar dehydroxylated surface and then comparing submonolayer coverages on the three different surfaces. This approach has been chosen because the coverage comparison showed no dependence on the type of surface and the substrate comparisons are most straightforward for the lower coverage.

4.1. TPD of $[Rh(CO)_2Cl]_2$ on porous and planar Al_2O_3

The TPD data for $[Rh(CO)_2Cl]_2$ on oxidized Al(100) (fig. 1) demonstrate two important points. First, the presence of the large zero order peak from cracking of $[Rh(CO)_2Cl]_2$ in the mass spectrometer shows that a condensed $[Rh(CO)_2Cl]_2$ layer can be formed. Second, the higher temperature peak from decomposition of $[Rh(CO)_2Cl]_2$ indicates that $[Rh(CO)_2Cl]_2$ decomposition is sensitive to the method of substrate preparation. The difference in CO evolution profiles for different substrates (fig. 1) was the subject of an XPS and TPD investigation in a previous paper [15]. At that time we were able to demonstrate a correlation between the CO evolution profile and the method of substrate preparation. That work also showed that the product of $[Rh(CO)_2Cl]_2$ decomposition is Rh particles whose size is very different on the two substrates: the porous substrate supported much smaller particles than did the planar support (20 Å versus 120 Å). By combining the TPD data with particle size estimates and XPS intensity we established the correlation between substrate porosity, Rh particle size, and decomposition profile. We also asserted that the differences in CO evolution profile showed a difference in decomposition mechanism, which in turn controlled the particle size that resulted after decomposition. In addition, we postulated that the molecular $[Rh(CO)_2Cl]_2$ was very mobile on the Al_2O_3 surface above the temperature at which condensed $[Rh(CO)_2Cl]_2$ desorbs. This allowed the molecule to diffuse to stable binding sites within the pore structure of the porous films which in turn lead to better dispersion of the precursor molecule over the surface and smaller resultant Rh particles. The HREELS data discussed below are more meaningful when seen in the context of this previous work of ours.

4.2. Comparison of different $[Rh(CO)_2Cl]_2$ coverages

Whenever one attempts to study a large condensable molecule such as $[Rh(CO)_2Cl]_2$ an understanding of the system must begin with the multilayer

condensed phase. If one can not understand the spectrum and behavior of the condensed molecule, when it will be very difficult to understand the chemisorbed layer. In these experiments all of the spectral features for the condensed multilayer $[Rh(CO)_2Cl]_2$ deposit (fig. 2a) were assigned in table 1 based on a combination of IR data for $[Rh(CO)_2Cl]_2$ in solution (CO stretching modes) and rhodium halogen compounds (Rh–Cl mode). For a multilayer deposit of sufficient thickness no lattice Al_2O_3 modes were observed making identification of the spectral features much easier. For $[Rh(CO)_2Cl]_2$ we found the condensed layer to remain on the surface up to a temperature of approximately 240 K, which was confirmed with TPD (fig. 1) and HREELS (fig. 2). As the condensed phase desorbs the peaks due to adsorbed $[Rh(CO)_2Cl]_2$ decline sharply and those due to the substrate Al_2O_3 increase in intensity. This behavior is expected since the surface $[Rh(CO)_2Cl]_2$ concentration decreases upon desorption of condensed $[Rh(CO)_2Cl]_2$.

After desorption of the condensed portion of the multilayer deposit (above 245 K in this case), a chemisorbed monolayer should remain on the surface. It would follow then that the spectrum obtained after desorption of the multilayer would be similar to that obtained by adsorption of a comparable monolayer coverage unless dissociation had already occurred. This comparison is made by examining fig. 2h and fig. 3c. Note that the CO stretching region is expanded to a higher degree in fig. 3. There is no valid method to compare absolute HREELS intensities between the two spectra; however, a qualitative comparison of relative intensities shows a that the data are very similar. From this we conclude that approximately a monolayer of $[Rh(CO)_2Cl]_2$ remains on the surface after desorption of the condensed phase.

In addition to the temperature dependent behavior of the $[Rh(CO)_2Cl]_2$ modes we also observe changes in the Al_2O_3 lattice modes. The most noticeable change that occured over the 245 to 275 K temperature range was in the apparent resolution of the Al_2O_3 lattice modes at 470 and 650 cm^{-1}. Prior to adsorption of $[Rh(CO)_2Cl]_2$ the Al_2O modes at 875, 650 and 470 cm^{-1} are clearly resolved; however, after $[Rh(CO)_2Cl]_2$ adsorption we observed an envelope between 450 and 1100 cm^{-1}. A similar effect was observed by Chen et al. when oxidized Al(100) was exposed to water to form surface hydroxyls [25]. They proposed that the formation of surface hydroxyl species preferentially attenuates the *surface* Al–O mode at 650 cm^{-1}. Similarly, we propose that $[Rh(CO)_2Cl]_2$ reacts with the Al_2O_3 surface to form Rh–O or Al–Cl bonds decreasing the amount of unbound surface Al–O species, therefore lowering the Al–O stretch intensity at 620 cm^{-1}. Thus, the attenuation of the 620 cm^{-1} mode shows a direct interaction of $[Rh(CO)_2Cl]_2$ with the surface oxygen atoms of the Al_2O_3 film. Data for Rh particles on oxidized Al(100) (formed by decomposition of $[Rh(CO)_2Cl]_2$) show that the average particle size increases at elevated temperature [15]; therefore, the amount of Rh

interacting directly with Al_2O_3 decreases. The effect of agglomeration at elevated temperatures is to increase the intensity of the 620 cm^{-1} mode.

4.3. Comparison of submonolayer $[Rh(CO)_2Cl]_2$ on porous and planar Al_2O_3

The primary motivation for this investigation was to confirm our conclusion that subsurface pores in the Al_2O_3 substrates played a major role in determining the $[Rh(CO)_2Cl]_2$ decomposition mechanism. In our previous study we conclude that $[Rh(CO)_2Cl]_2$ diffused to stable binding sites within the pore structure below the temperature at which decomposition occurred. Further, these sites within the pores stabilized significantly smaller particles than did the available sites on the more planar surfaces. The data that allow us to best discuss the issue of surface $[Rh(CO)_2Cl]_2$ mobility are the HREELS data for submonolayer $[Rh(CO)_2Cl]_2$ exposures of figs. 3 and 4. For a submonolayer deposits below 250 K no desorption of CO, for either $[Rh(CO)_2Cl]_2$ desorption or $[Rh(CO)_2Cl]_2$ decomposition, occurs. Since no CO is desorbing from the surface below 250 K, changes in the CO stretch monitor changes in the nature of the adsorbed $[Rh(CO)_2Cl]_2$ layer. Fig. 6 shows the CO stretch intensity, normalized to the intensity for the layer at 110 K, as a function of temperature for submonolayers of $[Rh(CO)_2Cl]_2$ on both porous and planar Al_2O_3. For both samples the CO stretch intensity increases between 110 and 200 K. Since the amount of $[Rh(CO)_2Cl]_2$ on the surface is constant over this temperature range then the increased intensity must be due to an ordering of the $[Rh(CO)_2Cl]_2$ monolayer. This effect is largest for $[Rh(CO)_2Cl]_2$ on the porous support, presumably because the increased surface roughness leads to a more disordered $[Rh(CO)_2Cl]_2$ layer at 110 K. For both surfaces no shift in the CO stretching frequency accompanies the intensity increase; therefore, reaction of $[Rh(CO)_2Cl]_2$ to dissociate or form other compounds is not likely.

The behavior of $[Rh(CO)_2Cl]_2$ on the two substrates differs strongly above 200 K. For the porous sample the CO stretch intensity drops linearly to zero by 240 K with no shift in the CO stretching frequency. From TPD (fig. 1) and HREELS data we know that decomposition of monolayer $[Rh(CO)_2Cl]_2$ occurs above 275 K; therefore, $[Rh(CO)_2Cl]_2$ is still adsorbed on the sample. Based on the TPD and HREELS results we conclude that surface $[Rh(CO)_2Cl]_2$ is mobile below 240 K and that it diffuses into the subsurface pores below 240 K. Once the $[Rh(CO)_2Cl]_2$ molecules leave the surface sites that are line-of-sight to the spectrometer they are no longer detectable by HREELS and thus the CO stretch disappears. We take this result as a direct observation of surface $[Rh(CO)_2Cl]_2$ mobility and as confirmation of the presence of subsurface pores on this Al_2O_3 film.

For $[Rh(CO)_2Cl]_2$ on the planar substrate two distinct regions in the CO stretch intensity versus temperature curve (fig. 6) are observed above 200 K.

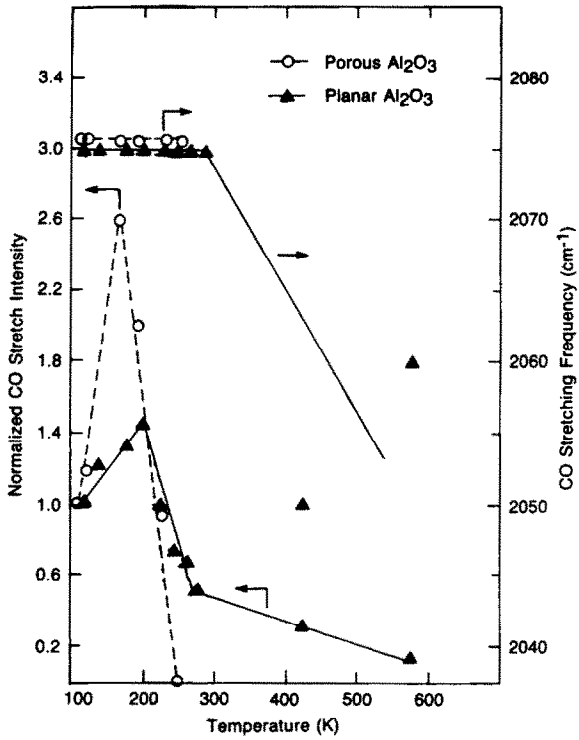

Fig. 6. Plot of the normalized CO stretch intensity versus temperature for submonolayers of $[Rh(CO)_2Cl]_2$ on porous and planar Al_2O_3. Results are taken from the spectra of figs. 3 and 5 and show the diffusion of $[Rh(CO)_2Cl]_2$ to subsurface sites on the porous Al_2O_3 overlayers.

Between 200 K and 275 K the CO intensity drops to about one third its maximum intensity followed by a continued decline above 275 K but with a greatly reduced slope. Also, in the temperature range between 275 and 575 CO stretching frequency shifts below 2080 cm^{-1} to to values near 2050–60 cm^{-1}. The measurable CO stretch intensity after annealing to 575 K is caused by readsorption of background CO during acquisition of the HREELS data. The decline in intensity above 275 K is easily understood because TPD (fig. 1) shows that CO is desorbed from the surface as a result of $[Rh(CO)_2Cl]_2$ decomposition. The frequency shift as a function of temperature tells us something about the nature of the CO adsorption sites above 275 K. Shifts in CO stretching frequency as a function of CO coverage are common for CO adsorption on transition metal surfaces. In this case the shift is to lower frequency as temperature is increased or as CO coverage is decreased in agreement with what is expected for CO on bulk metal samples. From this we conclude that CO is desorbing from large Rh particles mimicking CO desorp-

tion from bulk Rh samples. Formation of large Rh particles on planar Al_2O_3 samples was observed in our previous work where we concluded that these particles were formed by agglomeration of $[Rh(CO)_2Cl]_2$ into large crystallites at relatively low temperatures. This conclusion is supported by the decline in the CO stretch intensity between 200 and 275 K where no CO desorption is occurred but where $[Rh(CO)_2Cl]_2$ is very mobile on the surface. We interpret the sharp decline in intensity (fig. 6) in this region as being caused by agglomeration of $[Rh(CO)_2Cl]_2$ into large $[Rh(CO)_2Cl]_2$ crystallites with a resultant loss in $[Rh(CO)_2Cl]_2$ surface area. Since the CO stretching frequency is not changing in this region, we conclude that $[Rh(CO)_2Cl]_2$ is the mobile species as opposed to some other $Rh(CO)_2$ moiety.

4.4. Comparison of hydroxylated and dehydroxylated planar Al_2O_3

The importance and role of surface hydroxyl species in supported catalysts has been and continues to be a subject of frequent debate. In a conventional powdered Al_2O_3 sample the amount of surface hydroxyls is very large, and the addition of up to 10 wt% noble metal frequently has little change on their concentration or their IR spectrum. For this reason it is difficult to assess what importance they have to the activity of the catalyst. In a model catalyst such as the one examined in this paper the concentration of surface hydroxyls is comparable to the Rh concentration for a monolayer of $[Rh(CO)_2Cl]_2$. For this reason one might expect to be able to monitor the interaction of these two species on the surface. In a previous unpublished work we observed no effect of the addition of surface hydroxyls on the Rh particle size obtained by $[Rh(CO)_2Cl]_2$ decomposition to 575 K; however, that result was tainted by our limited ability to monitor the surface OH concentration by XPS. For oxide layers prepared in the manner shown here, surface charging during XPS broadens the O(1s) level so that resolution of the O(1s) shoulder from OH is questionable. HREELS offered a more solid identification of the presence of OH on the surface but it cannot quantify the surface OH concentration. The presence of hydroxyls for surface prepared by oxidation with water was confirmed by HREELS which also showed the OH groups to be stable to about 425 K in the absence of $[Rh(CO)_2Cl]_2$. Fig. 5 shows that the $[Rh(CO)_2Cl]_2$ interacted with the OH groups leading to a loss in O–H stretch intensity at 110 K, well below 425 K; however, we declined to speculate about the details of that interaction. For the comparison of the two substrates, however, the data indicate that the OH groups are present on the surface in sites that are accessible to the $[Rh(CO)_2Cl]_2$ molecules. Focusing now on the CO stretch, the temperature dependence of the data is very similar to that from the OH *free* surface. The main point is that the CO stretch intensity drops by less than 50% at 265 K followed by a gradual decline at higher temperatures in accordance with the expected CO evolution profile (fig. 1).

Unfortunately, the Rh–Cl region is obscured by the substrate lattice modes; it is this region we would suspect to be most effected by the inclusion of hydroxyls on the surface. These results are in agreement with our previous data which showed no major effect of OH on either the decomposition profile (fig. 1) or the resultant Rh particle size (120 Å for a planar surface). We are more than slightly hesitant to conclude that OH groups are unimportant for supported metal catalysts and can propose several explanations for the results we obtain. One strong possibility is that, although detectable by HREELS, the actual surface OH concentration is quite low for this model catalyst and therefore not involved with the majority of the $[Rh(CO)_2Cl]_2$.

Although the Rh–Cl stretch is obscured, the O–H stretching region is less affected by overlap with other losses; however, there is some interference with a harmonic of the Al_2O_3 lattice modes around 3500 cm^{-1}. When $[Rh(CO)_2Cl]_2$ was adsorbed, the O–H stretch was no longer detectable; and when the sample was annealed to elevated temperature, the original O–H stretch intensity was never regained. We take this behavior as indicative of an interaction of $[Rh(CO)_2Cl]_2$ with the surface hydroxyls, presumably a reaction; but, a stronger statement is not warranted based on this data alone. One complication is that the O–H stretch region always shows some intensity which is partially due to the Al–O harmonics but must contain some other components. This leads to a broad peak around 3700 cm^{-1} which is not as clearly resolved as the O–H stretch from the clean Al_2O_3 film.

4.5. Usefulness of HREELS for studies on oxide supports

Aside from the questions raised about the interaction of $[Rh(CO)_2Cl]_2$ with Al_2O_3, these experiments also offer an excellent test case for HREELS on oxide supports. In particular, $[Rh(CO)_2Cl]_2$ is a good molecule to challenge the resolution and detection capabilities of HREELS under these less than optimal conditions. The IR spectrum of $[Rh(CO)_2Cl]_2$ is known to have a doublet at about 2100 cm^{-1} from the symmetric and asymmetric stretch of dicarbonyl CO. Also, the low wavenumber modes from Rh–Cl and Rh–CO should be detectable; these modes are usually not observed by conventional IR spectroscopy. The data show that all of these expected modes are observed for a multilayer deposit on Al_2O_3; however, not for the more chemically interesting case of the submonolayer deposit.

When submonolayers of $[Rh(CO)_2Cl]_2$ are examined, several complications arise to make the data less than optimal. First, the low wavenumber $[Rh(CO)_2Cl]_2$ modes are obscured by the very strong lattice Al_2O_3 modes. These vibrations, with detectable harmonics to 3000 cm^{-1}, are the dominant peaks in the spectrum and prohibit monitoring of Rh–Cl bond scission. Hence, interference of the substrate vibrational modes limits the use of the

region below 1000 cm^{-1}. The situation may be improved by using a different method for preparation of the oxide support. If the oxide were much thinner (e.g., less than 10 Å), then these modes could be severely reduced in intensity. Thin oxide layers may show weaker lattice modes if the long range order of the oxide lattice is disrupted. For the experiments presented here thin layers were not practical because of migration of metallic Al to the surface at elevated temperature. Metallic Al was observed by us to cause chemistry unrepresentative of Al_2O_3, in that it induced substantial amounts of CO dissociation not observed on the thicker Al_2O_3 layers. This problem may be avoided by growing thin Al_2O_3 layers on a refractive substrate such as molybdenum, thereby eliminating the essentially infinite reservoir of reduced Al present for Al_2O_3 layers on Al(100). Thus, preparation of thin Al_2O_3 layers on a substrate other than Al eliminates the problem of interference from metallic Al and may extent the range of useful HREELS down to 300 cm^{-1}.

The other limitation to the HREELS data obtained from oxides is the resolution. Typically, HREELS has a resolution, defined as the FWHM of the elastic peak, of about 40 cm^{-1}, with the best resolution obtained for very clean and well ordered single crystal samples. When one switches to an oxide surface with undetermined long range order, it is expected that the data quality would degrade somewhat. That was observed for these samples where the best resolution on the elastic peak obtainable was about 65 cm^{-1}. The practical implication of this degraded resolution can be seen by examining the C–O stretching region for any of the samples. As we stated before the expected symmetric and asymmetric stretch for the dicarbonyl Rh could not be resolved in any of the data. The question is: are these peaks resolvable HREELS even under optical conditions, say for CO on a single crystal Rh sample? Assuming that the separation of the peaks is 80 cm^{-1} and using the width usually obtained for liner CO on Rh(100), we conclude that our spectrometer could detect two loss peaks that overlap at about 65% of their maximum. Thus, HREELS has the ability to resolve the peaks under optimal conditions, but the oxide support restricts our resolution of those peaks in this case. In spite of the limited resolution to overall width of the peak at 2080 cm^{-1} (i.e., fig. 2c) shows that it is composed of more than one peak. We expect that the resolution will improve also when we change to the thinner Al_2O_3 support.

Above we listed two limitations on the quality of HREELS obtained from the oxide surface. This is not to say however that HREELS is useless for the study of oxide systems. This paper presents a clear example of how HREELS can give insight into the reaction of a relatively complex molecule with Al_2O_3. Work by Chen et al. [31] has shown that HREELS can be applied to CO adsorbed on Ni particles supported on Al_2O_3 films prepared in a similar manner to those shown here. These are just two examples of good experimental information obtained with HREELS from oxide supported metals. By making the Al_2O_3 substrates much thinner and also free of metallic Al, the

HREELS results from these samples should improve to the point where more subtle and informative HREELS results are possible.

5. Summary

We have studied the interaction of $[Rh(CO)_2Cl]_2$ with three different Al_2O_3 supports using HREELS and TPD to understand the decomposition mechanism for this class of catalyst precursor. HREELS measurements showed that adsorbed $[Rh(CO)_2Cl]_2$ is very mobile between 200 and 240 K, allowing $[Rh(CO)_2Cl]_2$ to diffuse to more stable adsorption sites on the Al_2O_3 surfaces. For the porous surfaces the presence of a large number of relatively stable binding sites within the subsurface pores leads to a high dispersion of $[Rh(CO)_2Cl]_2$ and therefore small Rh particles [15]. On the planar Al_2O_3 substrates relatively few high binding energy $[Rh(CO)_2Cl]_2$ adsorption sites are present; therefore, the very mobile $[Rh(CO)_2Cl]_2$ agglomerates into large $[Rh(CO)_2Cl]_2$ crystallites and forms large Rh particle upon subsequent decomposition. These results demonstrate the importance of the substrate in controlling Rh particle size for supported Rh particles while confirming the mechanism proposed earlier [15] to explain the substrate dependence of $[Rh(CO)_2Cl]_2$ decomposition.

Data for adsorption of $[Rh(CO)_2Cl]_2$ onto hydroxylated Al_2O_3 films were also obtained showing an interaction of $[Rh(CO)_2Cl]_2$ with surface OH species. After annealing an adsorbed $[Rh(CO)_2Cl]_2$. The experiments also show that HREELS can be useful for the study of model catalysts such as the one prepared. Although the resolution is degraded by about 60% compared to ideal conditions for HREELS, useful vibrational data were still obtained for Rh supported on Al_2O_3.

References

[1] K.C. Taylor, in: Vol. 30 of Studies in Surface Science and Catalysis, Eds. A. Crucq and A. Frennet (Elsevier, Amsterdam, 1987) p. 97.
[2] K.C. Taylor, Automobile Catalytic Convertors (Springer, Berlin, 1984).
[3] R.K. Herz, E.J. Shinouskis, A. Dayte and J. Schwank, Ind. Eng. Chem. Prod. Res. Develop. 24 (1985) 6.
[4] K.C. Taylor and R.M. Sinkevitch, Ind. Eng. Chem. Prod. Res. Develop. 22 (1983) 45.
[5] S.H. Oh, G.B. Fisher, J.E. Carpenter and D.W. Goodman, J. Catalysis 100 (1986) 360.
[6] D.W. Goodman, Surface Sci. 123 (1982) L679.
[7] C.H.F. Peden and D.W. Goodman, J. Catalysis 104 (1987) 347.
[8] R.A. Dictor, J. Catalysis 109 (1988) 89.
[9] J.L. Roustan, Y. Lijour and B.A. Morrow, Inorg. Chem. 26 (1987) 2509.
[10] J.T. Yates, Jr., T.M. Duncan and R.W. Vaughan, J. Chem. Phys. 71 (1979) 3908.

[11] C.A. Rise, S.D. Worley, C.W. Curtis, J.A. Guinn and A.R. Tarrer, J. Chem. Phys. 74 (1981) 6487.
[12] Y.U. Yermakov, B.M. Kuznetsov and V.A. Zakharov, Catalysis by Supported Complexes (Elsevier, Amsterdam, 1981).
[13] G.S. McNully, K. Cannon and J. Schwartz, Inorg. Chem. 25 (1986) 25.
[14] D.G.H. Ballard, Advan. Catalysis 23 (1973) 263.
[15] D.N. Belton and S.J. Schmeig, Surface Sci. 199 (1988) 518.
[16] P.M. Lausarot, G.A. Vaglio and M. Valle, J. Organometal. Chem. 204 (1981) 249.
[17] A.K. Smith, F. Hughes, A. Theolier, J.M. Basset, R. Ugo, G.M. Zanderighi, J.L. Bilhou, V. Bilhou-Bougno. and W.F. Graydon, Inorg. Chem. 18 (1979) 3104.
[18] G.C. Smith, T.P. Chojnacki, S.R. Dasgupta, K. Iwatate and K.L. Watters, Inorg. Chem. (1975) 1419.
[19] W.M. Bowser and W.H. Weinberg J. Am. Chem. Soc. 103 (1981) 1453.
[20] B.G. Frederick, G. Apai and T.N. Rhodin, J. Am. Chem. Soc. 109 (1987) 4797.
[21] B.A. Sexton, J. Vacuum Sci. Technol. 16 (1979) 1033.
[22] D.N. Belton and S.J. Schmieg, Appl. Surface Sci. 32 (1988) 173.
[23] F.J. Szalkowski, J. Chem. Phys. 77 (1982) 5224.
[24] E.D. Johnson, PhD Thesis, Cornell University, 1985.
[25] J.G. Chen, J.E. Crowell and J.T. Yates, Jr., J. Chem. Phys. 84 (1986) 5906.
[26] D.L. Cocke, E.D. Johnson and R.P. Merrill, Catalysis Rev.-Sci. Eng. 26 (1984) 163.
[27] D.N. Belton and S.J. Schmieg, unpublished results.
[28] J.L. Erskine and R.L. Strong, Phys. Rev. B 25 (1982) 5547.
[29] R.L. Strong, B. Firey, F.W. de Wette and J.L. Erskine, Phys. Rev. B 26 (1982) 3483.
[30] C.W. Garland and J.R. Wilt, J. Chem. Phys. 36 (1962) 1094.
[31] J.G. Chen, J.E. Crowell and J.T. Yates, Jr., Surface Sci. 187 (1987) 80.
[32] M.A. Bennett, R.J.H. Clark and D.L. Milner, Inorg. Chem. 6 (1967) 1647.